Mandy Esch
Vladimir L. Sukhorukov
Markus Kürschner
Ulrich Zimmermann
Lehrstuhl für Biotechnologie der Universität Würzburg, Biozentrum, Am Hubland, D97074 Würzburg, Germany

Received 22 October 1998; accepted 2 February 1999

Dielectric Properties of Alginate Beads and Bound Water Relaxation Studied by Electrorotation

Abstract: *The electrical and dielectric properties of Ba^{2+} and Ca^{2+} cross-linked alginate hydrogel beads were studied by means of single-particle electrorotation. The use of microstructured electrodes allowed the measurements to be performed over a wide range of medium conductivity from about 5 mS/m to 1 S/m. Within a conductivity range, the beads exhibited measurable electrorotation response at frequencies above 0.2 MHz with two well-resolved co- and antifield peaks. With increasing medium conductivity, both peaks shifted toward higher frequency and their magnitudes decreased greatly. The results were analyzed using various dielectric models that consider the beads as homogeneous spheres with conductive loss and allow the complex rotational behavior of beads to be explained in terms of conductivity and permittivity of the hydrogel. The rotation spectra could be fitted very accurately by assuming (a) a linear relationship between the internal hydrogel conductivity and the medium conductivity, and (b) a broad internal dispersion of the hydrogel centered between 20 and 40 MHz. We attribute this dispersion to the relaxation of water bound to the polysaccharide matrix of the beads. The dielectric characterization of alginate hydrogels is of enormous interest for biotechnology and medicine, where alginate beads are widely used for immobilization of cells and enzymes, for drug delivery, and as microcarriers for cell cultivation.* © 1999 John Wiley & Sons, Inc. Biopoly 50: 227–237, 1999

Keywords: *alginate beads; hydrogel; dielectric spectroscopy; dispersion; bound water; electrorotation*

INTRODUCTION

Polysaccharides from marine algae, alginates, have found a variety of medical and biotechnological applications based on their strong ability to form stable hydrogels in the presence of some multivalent cations. Due to their excellent biocompatibility, purified alginates are widely used for immobilization of cells and enzymes,[1] immunoisolated transplantation of cells and tissues,[2–5] wound dressing, and drug delivery.[6–9] Recently, new

Correspondence to: Prof. Dr. U. Zimmermann; email: zimmermann@biozentrum.uni-wuerzburg.de
Contract grant sponsor: Deutsche Forshungsgemeinschaft (DFG) and BMBF
Contract grant number: SFB 176, project B5 (DFG) and BEO 22-0311347 (BMBF)
Biopolymers, Vol. 50, 227–237 (1999)

CCC 0006-3525/99/030227-11

microcarriers suitable for large-scale cultivation of anchorage-dependent mammalian cells have been developed by coating barium-alginate beads with collagen.[10] Very fragile mammalian cells, plant protoplasts, and tissues (e.g., islets of Langerhans[11,12] and parathyroid tissue[13]) can be immobilized by entrapping them in alginate gel microspheres, because this procedure is carried out in a single step under very mild conditions. The implementation of this immobilization technique is very simple. Cells are suspended in a sodium alginate solution, and the mixture is dripped into a precipitation solution containing Ca^{2+} or Ba^{2+} ions.[14] Gelation of the droplets occurs instantaneously via ionotropic mechanism, entrapping the cells within the three-dimensional matrix of the ionically cross-linked polymer.

The functional properties of alginate hydrogel as a cell immobilization matrix strongly correlate with the chemical composition and structure of the polysaccharide, which, in turn, depend on the species of alga from which it is isolated.[7,8,15] Alginates are linear polysaccharides composed of homopolymeric regions of mannuronic and guluronic acids (M and G blocks) interspaced with regions of alternating structure (MG blocks). The gel-forming ability of alginates was found to be closely related to the content of G residues and to the length of G blocks.[7] Stable alginate beads with a homogeneous pore size distribution (i.e., with an uniform radial distribution of the polymer concentration) can be produced if beads are formed in the presence of nongelling cations, such as Na^{+} or Mg^{2+} (see Materials and Methods). Otherwise, alginate beads with a capsular structure are produced with a narrower network on the bead surface than in the gel core.[15,16] It is evident that the porosity of alginate gels is essential for the diffusion-driven molecular transport of nutrients and cell metabolites, and therefore for the viability and function of entrapped cells.[6]

However, the diffusion characteristics of alginate hydrogel as well as other physicochemical properties of this material cannot be completely explained without regarding its electrical and dielectric parameters. These properties are of relevance for electrostatic interactions and therefore for the effective pore size and for the diffusion rate of charged species within the polyanionic alginate matrix. Furthermore, dielectric measurements over a wide frequency range can also provide valuable information on structural characteristics and microenvironment of complex polymer systems, such as mobility of charged molecular groups and dipoles,[17] content and physical state of water,[18,19] which in turn determine the rate of chemical reactions and enzyme activity,[20] etc. Whereas the dielectric data of alginate *solutions* are available in the literature,[21,22] the dielectric and electrical properties of alginate hydrogels have not been studied yet. This kind of data can be obtained from the traditional impedance measurements on densely packed alginate beads with the disadvantages that the method is restricted to low-conductivity solutions because of the electrode polarization processes and that the hydrogel properties must be deduced from sophisticated mixture equations.[23–25]

An alternative approach to the study of the dielectric properties of biological and polymer particles is the single-particle electrorotation technique.[26] In the last few years, electrorotation has become the principal means used not only for the dielectric characterization of biological cells and polymer particles[27–30] but also for studying the ion transport phenomena in living cells.[31–33] In this study we found that alginate hydrogel microspheres (with radius of 40–100 μm) were ideal objects for electrorotation measurements. From electrorotation spectra recorded at various external conductivities, the values for conductivity and permittivity of the hydrogel could be derived using theoretical methods based on the dipole models that have been well tested for other complex biological and polymer particles.[30,31] Within a conductivity range, the rotation spectra of beads exhibited two separate rotational peaks, one of which was due to the Maxwell–Wagner polarization at the interface bead–external solution, whereas the second peak was caused by internal dielectric dispersion of the beads. This dispersion was centered in the MHz frequency range and arose mainly from the relaxation of bound water.

THEORY

General

Electrorotation of microscopic particles as well as other phenomena of AC electromechanics, such as dielectrophoresis, electrodeformation, etc., is based on the interaction between a time-varying electric field $\boldsymbol{E}$ with the electrical dipole μ induced by the field within the particle.[30,33,34] The induced dipole arises from the free charges that accumulate at the interface of the particle if its electrical properties differ from those of the suspending medium. For spherical particles subjected to alternating or rotating electric fields, the induced dipole is a complex function of the field frequency f[19,28,35,36]:

$$\boldsymbol{\mu} = 4\pi a^3 \varepsilon_e \cdot \boldsymbol{E} \cdot \left(\frac{\varepsilon_i^* - \varepsilon_e^*}{\varepsilon_i^* + 2\varepsilon_e^*} \right) \tag{1}$$

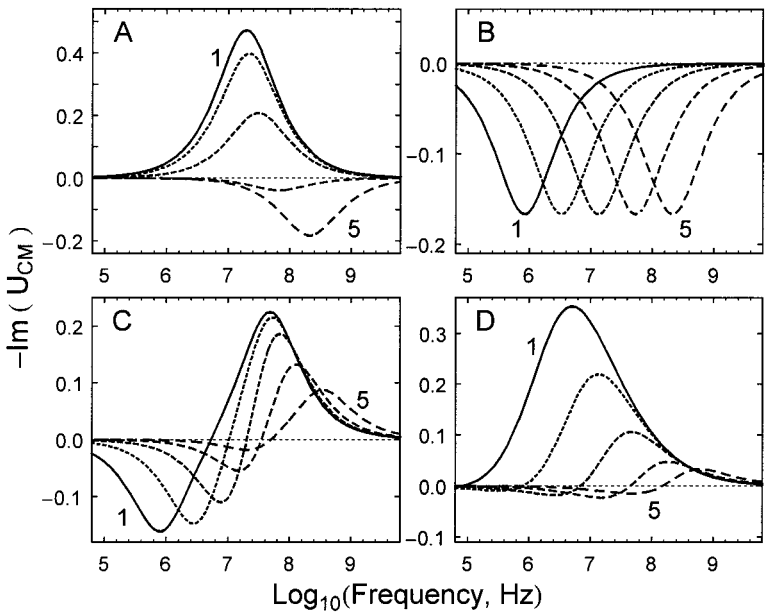

FIGURE 1 Theoretical rotation spectra for homogeneous spherical particles calculated on the basis of models 1–4 (A–D) in aqueous suspension media ($\varepsilon_e = 80$) of varied conductivity $\sigma_e = 5$ (curve 1), 20 (2), 80 (3), 320 (4), and 1280 mS/m (5). The spectra are represented by the imaginary part of the Clausius–Mosotti function $U^*_{CM} = (\varepsilon_i^* - \varepsilon_e^*)/(\varepsilon_i^* + 2\varepsilon_e^*)$, see Eq. (3). A, model 1, combination of Eqs. (2) and (3): nondispersive particle with invariable parameters $\varepsilon_i = 80$ and $\sigma_i = 250$ mS/m. B, model 2, Eqs. (2) and (3): nondispersive particle with $\varepsilon_i = 80$ and $\sigma_{il} = 0.25 \cdot \sigma_e$, i.e., the internal conductivity is directly proportional to that of the suspension medium. C and D, models 3 and 4, Eqs. (2), (3), and (5): dispersive particles with $\varepsilon_{il} = 80$, $\varepsilon_{ih} = 5$, $\sigma_{il} = 0.25 \cdot \sigma_e$, and a dispersion centered at $f_d = 31.8$ MHz (corresponding to a time constant of $\tau_d = 5$ ns). A single relaxation time ($\alpha = 1$, C) and a broad distribution of relaxation times ($\alpha = 0.3$, D) were assumed (see also Figure 3). Note that only the dispersive model (C and D) accounts for the appearance of two peaks in the rotational spectra of homogeneous spheres. Refer to FIGURE 2 for the plots of the field frequencies giving rise to fastest rotation (f_C) vs the external conductivity for these models.

where a is the radius of the particle, ϵ_e is the permittivity of the medium, $(\varepsilon_i^* - \varepsilon_e^*)/(\varepsilon_i^* + 2\varepsilon_e^*)$ is the complex Clausius–Mosotti function U^*_{CM}. The parameters ε_i^* and ε_e^* are the complex permittivities of the particle and the external medium, respectively. For nondispersive dielectric particles and media with conductive loss, the complex permittivity is defined as:

$$\varepsilon^* = \varepsilon - j\sigma/\omega \tag{2}$$

where $j \equiv (-1)^{1/2}$, $\omega = 2\pi f$ is the radian field frequency, ε (real permittivity) and σ (real conductivity) are given in [F/m] and [S/m], respectively.

The torque acting on the particle results from the vector cross product between field and dipole, so that only the imaginary component of the dipole (i.e., of the Clausius–Mosotti function) contributes to the electrorotation response of the particle. In the steady state, the frequency-dependent rotation speed $\Omega(f)$, which results from the balance between the torque and the viscous drag, is related to U^*_{CM} as follows[19,27,28,30]:

$$\Omega(f) = -\frac{\varepsilon_e \boldsymbol{E}^2}{2\eta} \operatorname{Im}\left(\frac{\varepsilon_i^* - \varepsilon_e^*}{\varepsilon_i^* + 2\varepsilon_e^*}\right) \tag{3}$$

where η is the dynamic viscosity of the medium. In practice, the rotation spectra should be corrected by a scaling constant that accounts for the local field strength, frictional force, and electrode geometry.[31]

In order to determine the dielectric properties of the hydrogels, we tested whether the rotational behavior of alginate microbeads followed one of the theoretical models given below (models 1–4). The electrorotation spectra calculated using the theoretical models were plotted for several values of medium conductivity σ_e (Figure 1). In addition, the conductivity dependence of the field frequency giving maximum torque was calculated (f_C, Figure 2) for each

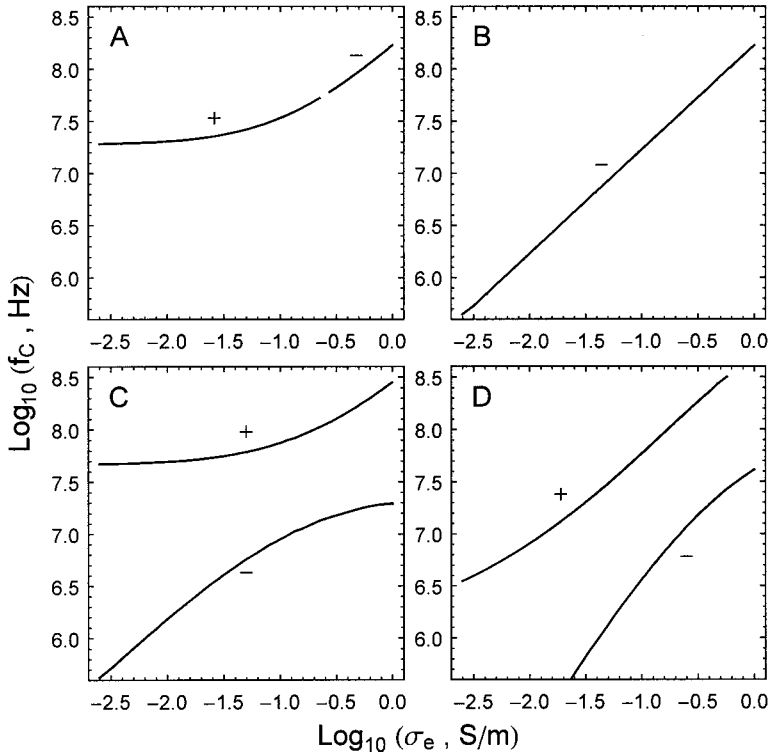

FIGURE 2 Theoretical double-logarithmic plots of the characteristic field frequencies (f_C) that induce fastest electrorotation vs the external conductivity σ_e. The dielectric parameters of particles were assumed to be identical to those used in Figure 1. The cofield and antifield rotational maxima are represented by the positive (+) and negative (−) branches of the curves, respectively.

model using the same σ and ε values used to plot the spectra in Figure 1. In the frequency range from few Hz to about 200 MHz available for electrorotation measurements, the dielectric properties of the suspension (aqueous) media were assumed to be frequency independent ($\varepsilon_e = 80 \cdot \varepsilon_0$), because the dispersion of water occurs at much higher frequency of about 20 GHz[18,37,38] (see also Figure 3).

The Dielectric Models

Nondispersive Particles (Models 1 and 2). Figures 1A and 1B show the theoretical electrorotation spectra calculated for homogeneous spheres with frequency-independent ε_i and σ_i in suspension media of varied conductivity σ_e. For both models, the field frequency giving maximum torque (f_C) shifts gradually to higher frequency with increasing external conductivity (Figures 2A and 2B). The curves in Figure 2 were generated from the points where the derivative of the rotation speed $\partial\Omega/\partial(f)$ [see Eq. (3)], with respect to field frequency is zero. In model 1 (Figures 1A and 2A), the value of ε_i is assumed to be equal to the permittivity of water $\varepsilon_i = \varepsilon_e = 80\ \varepsilon_0$ (because the total

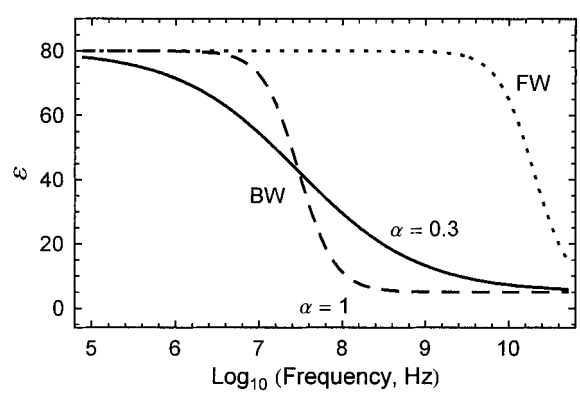

FIGURE 3 Frequency dependence of the permittivity ε originated from the principal relaxation of free water (FW, dotted line) at $f_d = 20$ GHz ($\varepsilon_l = 80$, $\varepsilon_h = 5$, $\alpha = 1$),[37,38,40] and that of bound water (BW) centered at much lower frequency. The curves for bound water were calculated by using Eq. (5a) and the following parameters: $f_d = 30$ MHz, $\varepsilon_l = 80$, $\varepsilon_h = 5$,$\alpha = 1$ (dashed line), and $\alpha = 0.3$ (solid line). Note, that these parameters are identical to those assumed for the dispersive particles, whose electrorotation response is shown in Figures 1C and 2C ($\alpha = 1$), and in Figures 1D and 2D ($\alpha = 0.3$).

water content in alginate hydrogels amounts to 98% of their mass),[6] and the value of σ_i is supposed to be independent of the medium conductivity. In the low-conductivity range (Figure 1A, $\sigma_e < \sigma_i$, curves 1–3), the particle exhibits cofield electrorotation, whereas if σ_e is higher than σ_i (Figure 1A, curves 4 and 5), antifield rotation is predicted by model 1. In model 2 (Figure 1B), we assumed that ion exchange occurs between the particle and the outer medium, and the σ_i value grows linearly with increasing salinity of the suspending medium. The spectra plotted using model 2 reveal only antifield rotation, because the particles are assumed to be less conductive than the medium ($\sigma_i/\sigma_e = 0.25$).

It is noteworthy that the rotational spectra of the homogeneous nondispersive spheres (models 1 and 2) exhibit only single peaks, which occur if the relaxation time of the Maxwell–Wagner interfacial polarization, $\tau_{MW} = (\varepsilon_i + 2\varepsilon_e)/(\sigma_i + 2\sigma_e)$, and field frequency match.[27,30] This rotation peak has the half-width of 1.14 decade of frequency and can be approximated by a Lorentzian curve[28]:

$$\Omega(f) = 2R\frac{f/f_C}{1 + (f/f_C)^2} \tag{4}$$

where the constant R combines $\boldsymbol{E}$, η, and all real conductivities and permittivities; the peak frequency f_C relates to the Maxwell–Wagner time constant as follows: $f_C = (2\pi \cdot \tau_{MW})^{-1}$.

Dispersive Particles (Models 3 and 4). In this study, two well-separated peaks were resolved in the rotation spectra of alginate beads if measurements were performed at relatively high external conductivities. These spectra could not be any longer explained by models 1 and 2, but they could be approximated very accurately by assuming an intrinsic dispersion of alginate hydrogel in the MHz-frequency range. The dispersion can be described by the following relations[39]:

$$\begin{cases} \varepsilon_i = \varepsilon_{ih} + \dfrac{\Delta\varepsilon_i}{1 + (\omega\tau_d)^{2\alpha}} \\ \sigma_i = \sigma_{il} + \dfrac{\Delta\sigma_i(\omega\tau_d)^{2\alpha}}{1 + (\omega\tau_d)^{2\alpha}} \end{cases} \tag{5ab}$$

where $\tau_d = (2\pi f_d)^{-1}$ is the relaxation time and f_d is the characteristic frequency of the dispersion; $\Delta\varepsilon_i = (\varepsilon_{il} - \varepsilon_{ih})$ and $\Delta\sigma_i = (\sigma_{ih} - \sigma_{il})$ are the interrelated dielectric increments, $\tau_d = \Delta\varepsilon_i/\Delta\sigma_i$; ε_{ih} (σ_{ih}) and ε_{il} (σ_{il}) are the values of the permittivity (conductivity) at high (subscript "h") and low (subscript "l") frequencies. The distribution range of the dispersion frequencies depends on α. A single dispersion frequency is given by $\alpha = 1$ (model 3, Figures 1C and 2C). Introduction of a distribution of relaxation frequencies described by $\alpha < 1$ (model 4, Figures 1D and 2D) significantly improves the fit of the rotation spectra of alginate beads (see below). The frequency dependence of the permittivity ε_i can be calculated using Eq. (5a) by assuming $f_d = 30$ MHz, $\alpha = 1$, and $\alpha = 0.3$ (Figure 3, dashed and solid curves, respectively). The dispersion of free water ($f_d = 20$ GHz, $\alpha \approx 1$)[40] is also shown in Figure 3 (dotted line). In models 3 and 4, a linear relationship between the low-frequency (ionic) conductivity of the particles σ_{il} and the external conductivity σ_e, was assumed (i.e., $\sigma_{il} = 0.25 \cdot \sigma_e$ Figures 1C, 1D, 2C, and 2D).

MATERIALS AND METHODS

Production of Barium and Calcium Cross-Linked Alginate Microspheres

Alginate (Manugel GMB) was obtained from Kelco (London, UK). Alginate solution (2 or 2.5%, wt/vol) was prepared in 0.9% NaCl. The pH was adjusted to 7.2–7.4 with 0.1 N NaOH. For purification, the sodium-alginate solution was subsequently filtered using an air pressure filtration device (SM 16249; Sartorius, Göttingen, Germany) and cellulose nitrate filters with a pore size of 3, 0.8, and 0.45 μm. The solution was stored for up to 6 weeks at +4°C.

For the preparation of Ba^{2+} and Ca^{2+} cross-linked alginate microspheres, the sodium-alginate solution was transferred into a 1-mL syringe and injected by a motor-driven piston at a constant rate of 200 μL/min into the central channel of a homemade nozzle with an inner diameter of 100 μm. Alginate beads were formed by dripping the sodium-alginate solution into a precipitation solution containing 20 m*M* $BaCl_2$, or $CaCl_2$, 10 m*M* morpholinopropanesulfonic acid (Sigma, M-5162), and 0.72% NaCl (pH 7.3–7.4, 280–300 mosmol/kg).[10] As shown elsewhere (Ref. 6), the beads formed in the presence of the nongelling sodium cations reveal homogeneous polymer distribution. The use of an air jet of 10 L/min resulted in beads of diameter in the range 40–100 μm, which were suitable for electrorotation measurements. The beads were stored in the precipitation solution for 12–48 h.

Electrorotation Measurements

Before use, the beads were washed with and resuspended in rotation media of various conductivities but of the same osmolality of 280–300 mosmol/kg. The rotation media contained the precipitation solutions and appropriate amounts of inositol (Sigma, I-5125) to adjust the conductivity. The osmolality and conductivity were determined by using a

cryoscope (Osmomat 030, Gonotec, Berlin, Germany) and a digital conductometer (Knick, Berlin, Germany).

Electrorotation spectra were measured in a microstructured four-electrode chamber developed by G. Fuhr (Humboldt University, Berlin, Germany). The electrorotation chamber, which was made by semiconductor technology,[30] was arranged as a planar array of circular electrodes of 60 μm diameter, 1 μm thickness, and 300 μm electrode spacing. The electrode material was gold. The electrical properties and frequency response of the rotation chamber has been well characterized and described in details earlier.[39] The optimized rotation chamber (where the distance between transmission line termination and electrode tip was minimized) used in the present study and by other workers[36] does not show any significant resonance or field attenuation up to the maximum frequency of our generator. The use of microelectrodes enabled a large-scale variation of the medium conductivity from 5 mS/m to a high conductivity of 1 S/m. The electrodes were driven by four 90° phase-shifted, symmetrically rectangular signals from a computer-controlled pulse generator HP 8130A (Hewlett-Packard, Boeblingen, Germany) with 2.5–4.8 V_{PP} amplitude over the frequency range from 100 Hz to 150 MHz.

For each experiment, a sample of bead suspension (50–70 μL) was added to the rotation chamber, and a coverslip was placed gently over its center. The beads were observed using a BX 50 Olympus microscope (Hamburg, Germany), and their radii were determined with a calibrated ocular micrometer. The microscope was equipped with a high-resolution CCD video camera (SSC-M370CE, Sony, Cologne, Germany) connected to a video monitor (TC-1470, Panasonic, Matsushita, Japan). Electrorotation spectra were monitored by decreasing the field frequency in steps (5 frequency points per decade starting at 150 MHz). At each field frequency, the rotation speed of the beads (Ω) was determined using a stopwatch. Since the field is inhomogeneous in the neighborhood of other beads or of the electrodes, only lone beads located near the center of the chamber were measured. The rotation spectra were normalized to the driving field strength of 1 V_{PP}/100 μm in accordance with Eq. (3) and fitted using the *Mathematica* software.[41]

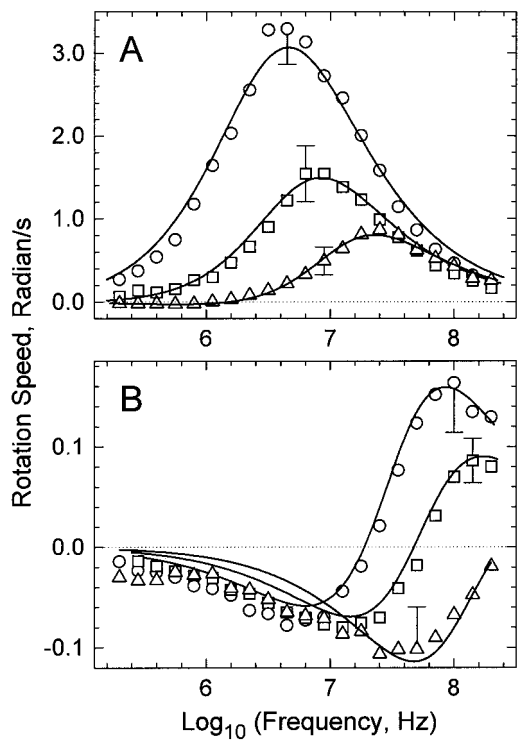

FIGURE 4 Experimental electrorotation spectra of 2%-Ba^{2+}-alginate beads measured at different external conductivities σ_e. A: 5 (○), 15 (□), and 50 (△) mS/m; B: 150 (○), 250 (□), and 500(△) mS/m, but of the same osmolality (300 mOsm). Each spectrum represents the mean (±SE) obtained from 3–9 particles. The curves are best fits of model 4 to the data. For the dielectric parameters used for curve fitting, see text and Table II. Note that at relatively high conductivities (e.g., B, 150 and 250 mS/m), the spectra exhibit two (anti- and cofield) rotation maxima. This rotational pattern fits the dispersive models, but it is not compatible with the nondispersive dielectric models.

RESULTS

Electrorotation Spectra of Gel Beads Formed from Ba^{2+}-(and Ca^{2+}-) Cross-Linked Alginate

The experimental electrorotation spectra for 2%-Ba^{2+}-alginate microbeads recorded at various external conductivities are shown in Figure 4. Under low-conductivity conditions ($\sigma_e < 50$ mS/m, Figure 4A), the beads exhibited a single cofield rotation peak with almost no deviation from the Lorentzian shape [Eq. (4)]. With increasing external conductivity, the cofield rotation peak given by the parameters f_{C1} and R_1 moved to higher frequencies, and an additional, well-resolved antifield peak (f_{C2} and R_2) appeared in the low-frequency part of the rotation spectra ($f_{C2} \ll f_{C1}$). These complex rotation spectra could be approximated accurately by a superposition of two Lorentzian curves, whose peak parameters determined by a least-square fitting procedure are listed in Table I. The magnitude of the cofield peak decreased rapidly from about 3 radian/s at 5 mS/m to 0.09 radian/s at 250 mS/m, whereas the antifield rotation speed grew gradually from 0.04 radian/s (at σ_e of 50 mS/m) to 0.3 radian/s (1 S/m). In accordance with the homogeneous particle models [Eq. (3)] the rotational peaks were insensitive to the radius a of the beads (data not shown). The hydrogel beads formed from 2.5%-Ba^{2+} and 2%-Ca^{2+}-cross-linked alginates also showed complex conductivity-dependent electrorotation be-

Table I The Parameters Obtained from Fitting the Superposition of Two Lorentzian Curves [Eq. (5)] to the Experimental Rotation Spectra of the Alginate Beads[a]

Alginate Beads	σ_e, S/m	n	Radius, μm	Cofield Peak		Antifield Peak	
				Log(f_{C1}, Hz)	R_1, rad/s	Log(f_{C2}, Hz)	R_2, rad/s
2% Ba^{2+}							
	0.005	9	37 ± 7	6.7 ± 0.1	3.03 ± 0.27		
	0.015	4	38 ± 2	6.9 ± 0.1	1.51 ± 0.19		
	0.05	8	38 ± 8	7.4 ± 0.1	0.64 ± 0.19	5.8 ± 0.1	−0.04 ± 0.02
	0.10	3	46 ± 8	7.7 ± 0.0	0.46 ± 0.04	6.4 ± 0.1	−0.08 ± 0.02
	0.15	5	37 ± 11	8.0 ± 0.2	0.17 ± 0.04	6.8 ± 0.2	−0.08 ± 0.01
	0.20	3	48 ± 7	8.1 ± 0.1	0.52 ± 0.53	6.9 ± 0.0	−0.33 ± 0.33
	0.25	5	33 ± 5	8.2 ± 0.1	0.09 ± 0.02	7.1 ± 0.1	−0.08 ± 0.01
	0.50	4	33 ± 9			7.6 ± 0.1	−0.12 ± 0.01
	1.0	4	37 ± 13			8.0 ± 0.1	−0.30 ± 0.14
2.5% Ba^{2+}							
	0.005	4	45 ± 10	6.9 ± 0.1	5.15 ± 1.02		
	0.015	4	50 ± 10	7.0 ± 0.0	2.98 ± 0.03		
	0.05	4	56 ± 7	7.5 ± 0.2	1.18 ± 0.30		
	0.15	4	42 ± 8	7.6 ± 0.7	0.36 ± 0.25	7.0 ± 0.6	−0.13 ± 0.03
	0.25	4	55 ± 7	8.2 ± 0.1	0.19 ± 0.02	7.0 ± 0.2	−0.14 ± 0.02
	0.50	4	38 ± 8			7.7 ± 0.2	−0.43 ± 0.47
	1.0	4	39 ± 5			8.1 ± 0.1	−0.14 ± 0.01
2% Ca^{2+}							
	0.015	5	40 ± 5	7.0 ± 0.1	2.24 ± 0.23		
	0.05	7	39 ± 9	7.3 ± 0.1	0.96 ± 0.20	5.8 ± 0.1	−0.02 ± 0.01
	0.10	5	43 ± 6	7.8 ± 0.1	0.35 ± 0.05	6.4 ± 0.1	−0.05 ± 0.01
	0.15	5	37 ± 5	7.9 ± 0.1	0.27 ± 0.02	6.6 ± 0.1	−0.05 ± 0.01
	0.25	6	51 ± 6	8.2 ± 0.1	0.12 ± 0.02	7.0 ± 0.2	−0.05 ± 0.00
	0.45	4	36 ± 1			7.7 ± 0.2	−0.12 ± 0.05

[a] n is the number of experiments. The data are normalized to the driving voltage of $1V_{PP}$ per 100 μm and represent the mean $\pm SD$.

havior, which was qualitatively similar to that of the 2%-Ba^{2+}-alginate (Table I).

Derivation of Dielectric Parameters from Rotation Data

Expressions for the electrorotational torque and the particle complex permittivity based on various dispersive and nondispersive models are given in the theory section. It is evident from the experimental data, particularly from the rotation spectra measured at high conductivities (Figure 4B), that models 1 and 2 are not consistent with the rotational behavior of alginate beads, because only one rotational peak is expected in the rotation response of *nondispersive* particles (see Figures 1A and 1B). The particles used in this study were homogeneous, and therefore the second peak in their rotational spectra can arise only due to an internal dispersion of the beads' material, i.e., due to the frequency dependence of the permittivity and conductivity of the hydrogel [Eq. (5)].

The dispersive models can explain the complexity of the rotation response of alginate beads in terms of the permittivity, conductivity, and other dielectric properties of the hydrogel, and allow these parameters to be deduced by fitting the theoretical models to the experimental rotation spectra. In practice, however, the simultaneous fitting of several rotational spectra taken at various conductivities by a model with at least five unknown variables (ε_{il}, ε_{ih}, σ_{il}, f_d, and α) is a difficult computation. Therefore we extracted the dielectric properties of the hydrogels from the conductivity dependence of the rotational peak frequencies f_{C1} and f_{C2}, as shown in Figure 5. The approach used here was to adjust the dielectric parameters (by varying them within realistic ranges) in order to achieve a subjective best fit of the theoretical peak frequency curves to the experimental data points. Similar fitting procedures were used elsewhere (Refs. 39 and 42) to extract the cellular dielectric properties from the characteristic frequencies of electroorientation and dielectrophoresis spectra of erythrocytes. We

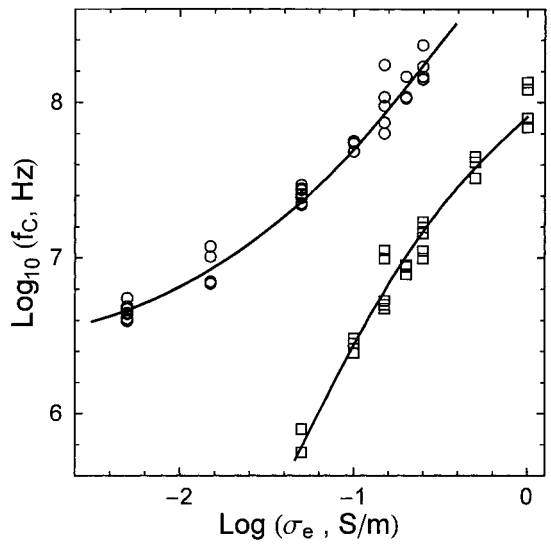

FIGURE 5 Cumulative double-logarithmic plot of the characteristic cofield (○) and antifield (□) frequencies vs the external conductivity. The data were obtained by fitting one Lorentzian curve [Eq. (4)], or a superposition of two Lorentzian curves to the rotational spectra of the Ba^{2+}-alginate beads shown in Figure 4 (see Table I). The solid curves are best fits of model 4 to the experimental data. The dielectric parameters derived by curve fitting for various alginate microbeads studied here are summarized in Table II.

found that the dispersive model with a single relaxation time (model 3, $\alpha = 1$) did not match the experimental electrorotation data on alginate beads obtained over the whole conductivity range. In contrast, introduction of the relaxation time spread parameter, $\alpha < 1$ (model 4), gave good agreement between the data and the theory (curves in Figure 5). This model implies a distribution of relaxation times or a superposition of overlapping relaxations that contribute to the complex dielectric response of the hydrogel. Figure 5 demonstrates the usefulness of model 4 for the analysis of the electrorotational data of alginate beads over the wide range of external conductivity used here.

Table II shows the dielectric parameters for alginate beads with different chemical composition deduced by fitting their f_C data. To achieve satisfactory fits, a linear relationship between the internal (σ_{il}) and the external conductivities (σ_e) had to be introduced. The dependence of the internal DC conductivity (i.e., ionic conductivity) on σ_e was expected, because the open lattice structure of the highly porous polymer matrix enables ion exchange to occur freely between the suspension medium and the hydrogel. Other dielectric parameters of the gels were assumed to be independent of the external conductivity.

The estimates of the dielectric parameters based on the f_C data (Figure 5) were then verified by fitting the experimental rotation spectra shown in Figure 4. The theoretical spectra (curves, Figure 4) were calculated using model 4 as well as the values for ε_{il}, ε_{ih}, σ_{il}, f_d, and α listed in Table II. To fit the theoretical spectra to the data, only a scaling factor (see theory section) for correction of field strength and friction was introduced. The good agreement of the experimental rotation spectra with the theoretical spectral curves is further justification of the validity of the dispersive particle model used here.

Dielectric Properties of Hydrogel Beads with Different Compositions

The electrorotation response (Figure 4, Table I) and therefore the dielectric parameters deduced for the hydrogel beads with various polysaccharide concentrations (2 and 2.5%) and cross-linking cations (Ba^{2+} and Ca^{2+}) were similar (Table II). The values of the low- and high-frequency internal permittivity (ε_{il} and ε_{ih}) were found in all cases to be close to those known for free bulk water and for bound hydration water ($\varepsilon_l = 80$ and $\varepsilon_h = 5$).[40] This result can be expected for particles, whose total water content is about 98%.[15] In addition, neither the nature of the cross-linking cation nor the concentration of alginate within the ranges used here had any noticeable influence on the mean dispersion frequency f_d and the relaxation time spread parameter α deduced from the rotation data. That the f_d value does not change distinctively, even as the internal conductivity σ_{il} varies greatly from about 1.2 mS/m to 250 mS/m (according to the relation $\sigma_{il} \approx 0.25 \cdot \sigma_e$ found here) as the external conductivity is increased from 5 mS/m to 1 S/m, indicates that this process is not due to the Maxwell–Wagner effect. This is because the parameters of the structural Maxwell–Wagner dispersions are strongly conductivity dependent.[19]

Table II Dielectric Properties of the Alginate Beads Extracted from the Experimental Data (Figures 4 and 5) Using Model 4

Parameter	2% Ba^{2+}	2.5% Ba^{2+}	2% Ca^{2+}
ε_{il}	70–100	70–80	80–90
ε_{ih}	5–10	6–8	11–13
σ_{il}/σ_e	0.20–0.25	0.15–0.20	0.28–0.30
α	0.20–0.22	0.20–0.30	0.18–0.22
f_d (MHz)	20–32	27–40	27–32

A slight decrease in the relative internal conductivity σ_{il} from (0.2–0.25) · σ_e to (0.15–0.20) · σ_e was observed for Ba^{2+}-alginate beads as the concentration of the polysaccharide was increased from 2 to 2.5%, respectively. This may have been due to a decrease of the porosity of the polymer matrix or to an increase of the viscosity of the hydration water, both of which can reduce the mobility of ions within the hydrogel with higher polysaccharide concentration.

DISCUSSION

Rotation Spectra

Although the nondispersive models match well the experimental spectra of alginate beads at low conductivities (Figure 4A), the occurrence of two rotational peaks at higher conductivities (Figure 4B) is inconsistent with this model. This demonstrated that rotation spectra must be taken at several conductivities before selecting or rejecting a model. The changes in the rotation spectra of beads with increasing conductivity could be modeled very well by assuming the dielectric properties of the hydrogel beads to be dependent on the field frequency. Since the alginate beads used here had homogeneous structure (see Materials and Methods), we are confident in assigning the second rotation peak to a dielectric dispersion of the hydrogel properties. From the rotation data, the dielectric parameters of the hydrogel (Table II) could be extracted, which are useful for its physicochemical characterization. The various alginate beads tested here exhibited an intrinsic dielectric dispersion centered between 20 and 40 MHz. Introduction of the relaxation time spread parameter significantly improved the fit of the dispersive particle model to the experimental rotation data.

The electrorotation response of alginate beads observed in this study differs from those of other polymer particles reported in the literature, such as latex,[27] Sephadex,[39] and polystyrene particles,[29] whose rotational spectra exhibit only single Lorentzian peaks in the kHz–MHz range and therefore can be fitted using nondispersive models. That the above polymer materials did not show intrinsic dispersions detectable by electrorotation may have been due to a lower dispersion strength ($\Delta\epsilon$), as compared to those of alginate hydrogels, as well as due to the limited conductivity and frequency ranges used by the workers. It is also noteworthy that in contrast to latex and polystyrene particles that exhibit "anomalous" electrorotation in the low-frequency region,[27,29] the alginate beads used here did not show any measurable rotation at frequencies below 10 kHz.

Mechanism of the Internal Dispersion

As already mentioned, the content of water in alginate beads is about 98%.[15] The dielectric activity of water can therefore be expected to dominate the dielectric response of the hydrogel. The data obtained by means of electrorotation (Table II) indicate clearly that the internal dispersion of alginate beads is mainly caused by the relaxation of water associated with the polymer matrix. It is well known that water molecules, when translationally immobilized, can still undergo rotational diffusion and therefore remain dielectrically active.[43,44] From the values of the dielectric increments ($\Delta\varepsilon = \varepsilon_{il} - \varepsilon_{ih}$) and relaxation frequencies (f_d, Table II), it can be concluded that almost all water entrapped within the hydrogels is bound, i.e., the water dipoles within alginate beads relax much slower than the dipoles of free bulk water do (see below). However, it must be noted that the derivation of gel hydration parameters from dielectric data is not straightforward and can lead to an overestimation of the volume excluded by the polymer, unless using the Wagner equation.[45] In addition, the density of hydration shells in a series of proteins has been found to be larger than that of free water, which is suggestive of a tightly packed bound water structure.[46] The conclusion about the high bound water content in alginate beads is also supported by the results obtained by means of the differential scanning calorimetry of various sugar alginate gels, where up to 90% of water is bound to the polysaccharides.[47] Other dispersion mechanisms, e.g. due to the relaxations of the counterions or polysaccharide chains do not appear to contribute significantly to the internal dispersion of alginate beads revealed by electrorotation. However, the possible existence of dispersions below the frequency range of bead rotation (Figure 4) cannot be excluded. Thus in alginate *solutions*, various counterions bound to the polysaccharide chains relax at the kHz–MHz frequencies (<1–5 MHz), giving rise to weak dispersions with the magnitudes of less than 10 dielectric units ($\Delta\varepsilon \leq 10$).[21] It is also unlikely that the internal dispersion of alginate hydrogel reported here was due to a Maxwell–Wagner relaxation based on structural inhomogeneities of the beads, because the dispersion frequency f_d was assumed to be independent of the conductivity.

Numerous studies using various time- and frequency-domain dielectric relaxation techniques have demonstrated that many water–polymer systems and biological materials exhibit dielectric dispersions in the MHz fre-

quency range and at lower frequencies.[19,38,48–50] These dispersions are often considered due to bound or hydration water, whose molecular dipoles relax at frequencies intermediate between bulk water (f_d = 20 GHz, $\tau_d \approx 8$ ps) and that of ice (~ 1 kHz, 0.2 ms).[38,43] Whereas the relaxation times of hydration water in solutions of low molecular weight organic compounds (amino acids, polyelectrolytes, etc.) are greater than that of bulk water only by a factor of 2–3,[18] the dielectric behavior of the high molecular weight biopolymers, such as DNA, proteins, etc., reveals a more dramatic shift of the bound water dispersion toward lower frequency, e.g., the bound water in *Escherichia coli* DNA relaxes at about 100 MHz.[51,52] In few cases, the dielectric spectra of water–polymer systems (e.g., gelatin– and polyvinylpyrrolidone–water systems),[50] show two readily distinguishable populations of water, one strongly and another weakly associated with the polymers. As a result of the discreteness of the dispersion, the amount of bound water can easily be evaluated from the increments of permittivity related to the bound water relaxations.

The values of the relaxation time spread parameter ($\alpha \approx 0.2–0.3$, Table II) reported here reveal that, in common with the majority of bound water systems,[17,19,38,53,54] a broad spectrum of time constants is involved in the dielectric relaxation response of water bound to alginate hydrogels. Figure 3 shows that this broad distribution of relaxation times results in a flatter slope of the permittivity dispersion curve as compared to that of normal bulk water, which is known to exhibit a nearly single-time relaxation ($\alpha \approx 1$).[38] Deviations from the single-time relaxation behavior is a common feature of solid and solid-like materials,[37,55] and therefore the spread of relaxation times in alginate hydrogels reported here can be expected, because gels are usually considered as porous solids with flexible walls.[56] As discussed elsewhere (Refs. 18 and 37), there should exist a distribution of relaxation times in any solid material, since the individual dipoles present in it (e.g., water dipoles in hydrogels) are not likely to reside in exactly the same environment, with some dipoles being more free to rotate than others.

In addition to the permittivity values, the internal conductivity of alginate beads was also determined from their electrorotation spectra. The low-frequency ionic conductivity of the hydrogels was smaller than that of the suspension solution by a factor of 3–7, indicating that the mobility of free ions within the hydrogel matrix is reduced with respect to that in bulk water. In the case of Ba^{2+}-alginate beads, the use of a more concentrated alginate solution resulted in a slight decrease of the ionic conductivity of the beads, which was presumably due to the reduced pore size within the hydrogel matrix. This result agrees with the structural data obtained on alginate gels using the small angle x-ray scattering technique.[16]

CONCLUSION

In this study the electrorotation technique has been proved to be able to yield important information about the high-frequency dielectric behavior of complex, cross-linked macromolecular systems containing bound water. The dipole-based electrorotational theory has been extended to include Ba^{2+}- and Ca^{2+}-cross-linked alginate microbeads, modeled as homogeneous conductive spheres with an intrinsic dielectric dispersion. The model provides an adequate explanation of the frequency- and conductivity-dependent electrorotational response of the hydrogel microbeads, and allows their dielectric and electrical properties to be determined. Evidence has been presented suggesting that alginate hydrogel displays a broad dispersion centered at 20–40 MHz, which is obviously dominated by the relaxation of water entrapped within the polysaccharide matrix. The data show that the dielectric and other related physical properties of water bound to alginate hydrogel, such as mobility, microviscosity, etc., differ significantly from those of normal bulk water. Knowledge of the dielectric relaxation phenomena in hydrogels is particularly interesting because it provides insight into the mechanisms of the dielectric dispersions in biological systems. Thus, it is reasonable to expect that some compartments of biological cells, e.g., cell walls and amyloplasts of plant cells (which are mostly formed from hydrophilic polysaccharide materials) and the protein rich cytoplasm of red blood cells, might exhibit similar dielectric behavior due to the polymer-bound water.

This work was supported by grants from the Deutsche Forschungsgemeinschaft (SFB 176, project B5) and from the BMBF (BEO 22-0311347) to UZ.

REFERENCES

1. Lanza, R. P.; Chick, W. L. Surgery 1997, 21, 1–9.
2. Clayton, H. A.; London, N. J. M.; Colloby, P. S.; Bell, P. R. F.; James, R. F. L. J Microencapsulation 1991, 8, 211–233.
3. Zimmermann, U.; Klöck, G.; Federlin, K.; Hannig, K.; Kowalski, M.; Brezel, R.G.; Horcher, A.; Entenmann, H.; Siebers, U.; Zekorn, T. Electrophoresis 1992, 13, 269–274.

4. Hallé, J.-P.; Bourassa, S.; Leblond, F. A.; Chevalier, S.; Beaudry, M.; Chapdelaine, A.; Cousineau, S.; Saintonge, J.; Yale, J.-F. Transplantation 1993, 55, 350–354.
5. Klöck, G.; Frank, H.; Houben, R.; Zekorn, T.; Horcher, A.; Siebers, U.; Wöhrle, M.; Federlin, K.; Zimmermann, U. Appl Microbiol Biotechnol 1994, 40, 638–643.
6. Smidsrød, O.; Skjåk-Bræk, G. Trends Biotechnol 1990, 8, 71–78. 7 Aslani, P.; Kennedy, R. A. J. Controlled Release 1996, 42, 75–82.
8. Rehm, B. H. A.; Valla, S. Appl Microbiol Biotechnol 1997, 48, 281–288.
9. Maysinger, D.; Morinville, A. Trends Biotechnol 1997, 15, 410–418.
10. Gröhn, P.; Klöck, G.; Zimmermann, U. Biotechniques 1997, 22, 970–975.
11. Lim, F.; Sun, A. M. Science 1980, 210, 908–910.
12. Zekorn, T.; Horcher, A.; Siebers, U.; Schnettler, R., Klöck, G.; Hering, B.; Zimmermann, U.; Bretzel, R. G.; Federlin, K. Acta Diabetologica 1992, 35(10), 99–106.
13. Hasse, C.; Klöck, G.; Zielke, A.; Schlosser, A.; Barth, P.; Zimmermann, U.; Rothmund, M. Int J Artif Organs 1996, 19, 735–741.
14. Gröhn, P.; Klöck, G.; Schmitt, J.; Zimmermann, U.; Horcher, A.; Bretzel, R. G.; Hering, B. J.; Brandhorst, D.; Brandhorst, H.; Zekorn, T.; Federlin, K. Exp Clin Endocrinol 1994, 102, 380–387.
15. Skjåk-Bræk, G.; Martinsen, A. In Seaweed Resources in Europe: Uses and Potentialp Guiry, M. D.; Blunden, G., Eds.; John Wiley & Sons: New York, 1991; pp 220–256.
16. Wang, Z. Y.; White, J. W.; Konno, M.; Saito, S.; Nozawa, T. Biopolymers 1995, 35, 227–238.
17. Hedvig, P. Dielectric Spectroscopy of Polymers; Adam Hilger: Bristol, 1977.
18. Pethig, R.; Kell, D. B. Phys Med Biol 1987, 32, 933–970.
19. Schwan, H. P. Ferroelectrics 1988, 86, 205–233.
20. Yoshioka, S.; Aso, Y.; Terao, T. Pharm Res 1992, 9, 607–612.
21. Ikeda, S.; Kumagai, H.; Nakamura, K. Carbohydr Res 1997, 301, 51–59.
22. Ikeda, S.; Kumagai, H. J Agric Food Chem 1997, 45, 3452–3458.
23. Kolde, G. T.; Carstensen, E .L. J Phys Chem 1976, 80, 55–59.
24. Schwan, H. P.; Takashima, S. In Encyclopedia of Applied Physics; Trigg, G. L., Ed.; VCH Publishers: Weinheim and New York, 1993; Vol 5, pp 177–200.
25. Gimsa, J.; Wachner, D. Biophys J 1998, 75, 1107–1116.
26. Arnold, W. M.; Zimmermann, U. Z Naturforsch 1982, 37c, 908–915.
27. Arnold, W. M.; Schwan, H. P.; Zimmermann, U. J Phys Chem 1987, 91, 5093–5098.
28. Jones, T. B. Electromechanics of Particles; Cambridge University Press: New York, 1995.
29. Zhou, X.-F.; Markx, G. H.; Pethig, R.; Eastwood, I. M. Biochim Biophys Acta 1995, 1245, 85–93.
30. Fuhr, G.; Zimmermann, U.; Shirley, S. G. In Electromanipulation of Cells; Zimmermann, U., Neil, G., Eds.; CRC Press: Boca Raton, FL, 1996; pp 259–328.
31. Sukhorukov, V. L.; Benkert, R.; Obermeyer, G.; Bentrup, F.-W.; Zimmermann, U. J Membrane Biol 1998, 161, 21–32.
32. Nielsen, K.; Schenk, W. A.; Kriegmeier, M.; Sukhorukov, V. L.; Zimmermann, U. Inorg Chem 1996, 35, 5762–5763.
33. Kürschner, M.; Nielsen, K.; Andersen, Ch.; Sukhorukov, V. L.; Schenk, W. A.; Benz, R.; Zimmermann, U. Biophys J 1998, 74, 3031–3043.
34. Sukhorukov, V. L.; Mussauer, H.; Zimmermann, U. J Membrane Biol 1998, 163, 235–245.
35. Arnold, W. M.; Zimmermann, U. J Electrostatics 1988, 21, 151–191.
36. Schnelle, T.; Müller, T.; Fuhr, G. Med Biol Eng Comput 1998, 36, in press.
37. Jonscher, A. K. In Dielectric Relaxation in Solids; Chelsea Dielectrics: London, 1983.
38. Hasted, J. B. In Aqueous Dielectrics; Chapman and Hall: London, 1973.
39. Gimsa, J.; Müller, T.; Schnelle, Th.; Fuhr, G. Biophys J 1996, 71, 495–506.
40. Pennock, B. E.; Schwan, H. P. J Phys Chem 1969, 73, 2600–2610.
41. Wolfram, S. The Mathematica Book, 3rd ed; Wolfram Media: Champaign, IL, 1996.
42. Miller, R. D.; Jones, T. B. Biophys J 1993, 64, 1588–1595.
43. Eisenberg, D.; Kauzmann, W. In The Structure and Properties of Water; Oxford University Press, London, 1969.
44. Jain, S. K.; Johari, G. P. J Phys Chem 1988, 92, 5851–5854.
45. Suzuki, M.; Shigematsu, J.; Kodama, T. J Phys Chem 1996, 100, 7279–7282.
46. Wei, Y.-Z.; Kumbharkhane, A. C.; Sadeghi, M.; Sage, J. T.; Tian, W. D.; Champion, P. M.; Sridhar, S.; McDonald, M. J. J Phys Chem 1994, 98, 6644–6651.
47. Gerdes, D. L.; Burns, E. E.; Harrow, L. S. Lebensm-Wiss Technol 1987, 20, 282–286.
48. Mashimo, S.; Kuwabara, S.; Yagihara, S.; Higasi, K. J Phys Chem 1987, 91, 6337–6338.
49. Teramoto, A.; Gu, H.; Miyazaki, Y.; Sorai, M.; Mashimo, S. Biopolymers 1995, 36, 803–810.
50. Yoshioka, S.; Aso, Y.; Otsuka, T.; Kojima, S. J Pharm Sci 1995, 84, 1072–1077.
51. Kuwabara, S.; Umehara, T.; Mashimo, S.; Yagihara, S. J Phys Chem 1988, 92, 4839–4841.
52. Mashimo, S.; Umehara, T.; Kuwabara, S.; Yagihara, S. J Chem Phys 1989, 93, 4963–4967.
53. Mashimo, S. Nozaki, R. Yagihara, S. Takeishi, S. 1982, J Chem Phys 77(12), 6259–6262.
54. Shinyashiki, N.; Asaka, N.; Mashimo, S. J Chem Phys 1990, 93, 760–764.
55. Strobl, G. In The Physics of Polymers; Springer: Berlin, 1996.
56. Belton, P. S. Int J Biol Macromol 1997, 21, 81–88.